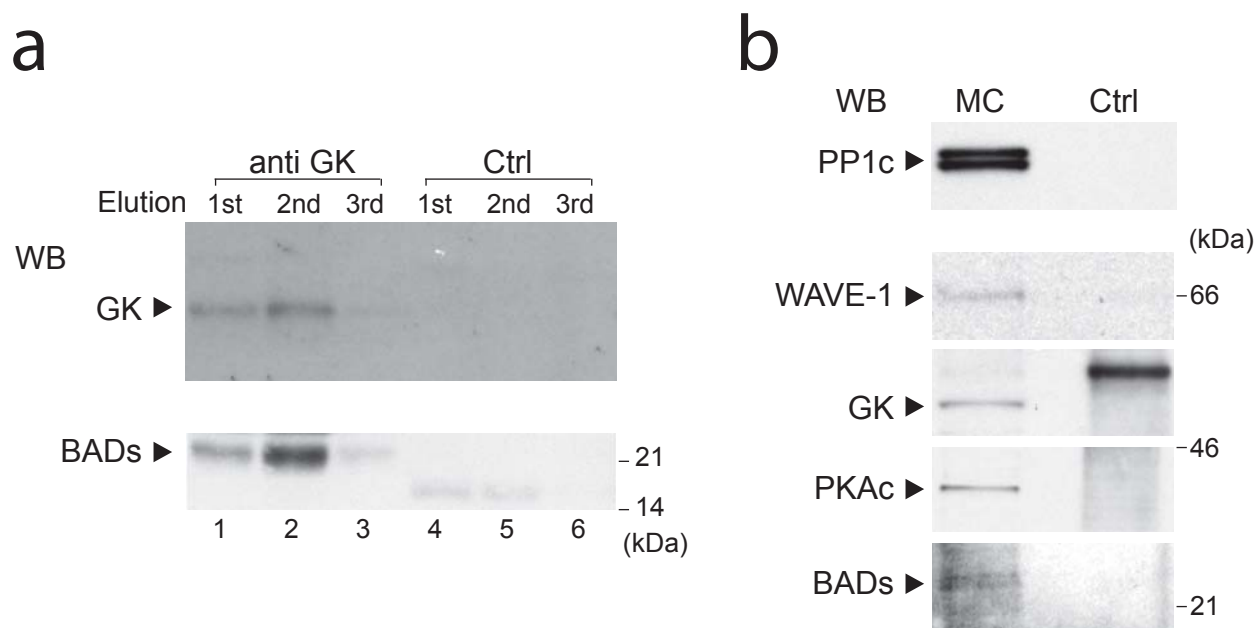# Dual Role of Pro-apoptotic BAD in Insulin Secretion and beta Cell Survival

Nika N. Danial, Loren D. Walensky, Chen-Yu Zhang, Cheol Soo Choi, Jill K. Fisher, Anthony J. A. Molina, Sandeep Robert Datta, Kenneth L. Pitter, Gregory H. Bird, Jakob D. Wikstrom, Jude T. Deeney, Kirsten Robertson, Joel Morash, Ameya Kulkarni, Susanne Neschen, Sheene Kim, Michael E. Greenberg, Barbara E. Corkey, Orian S. Shirihai, Gerald I. Shulman, Bradford B. Lowell, Stanley J. Korsmeyer
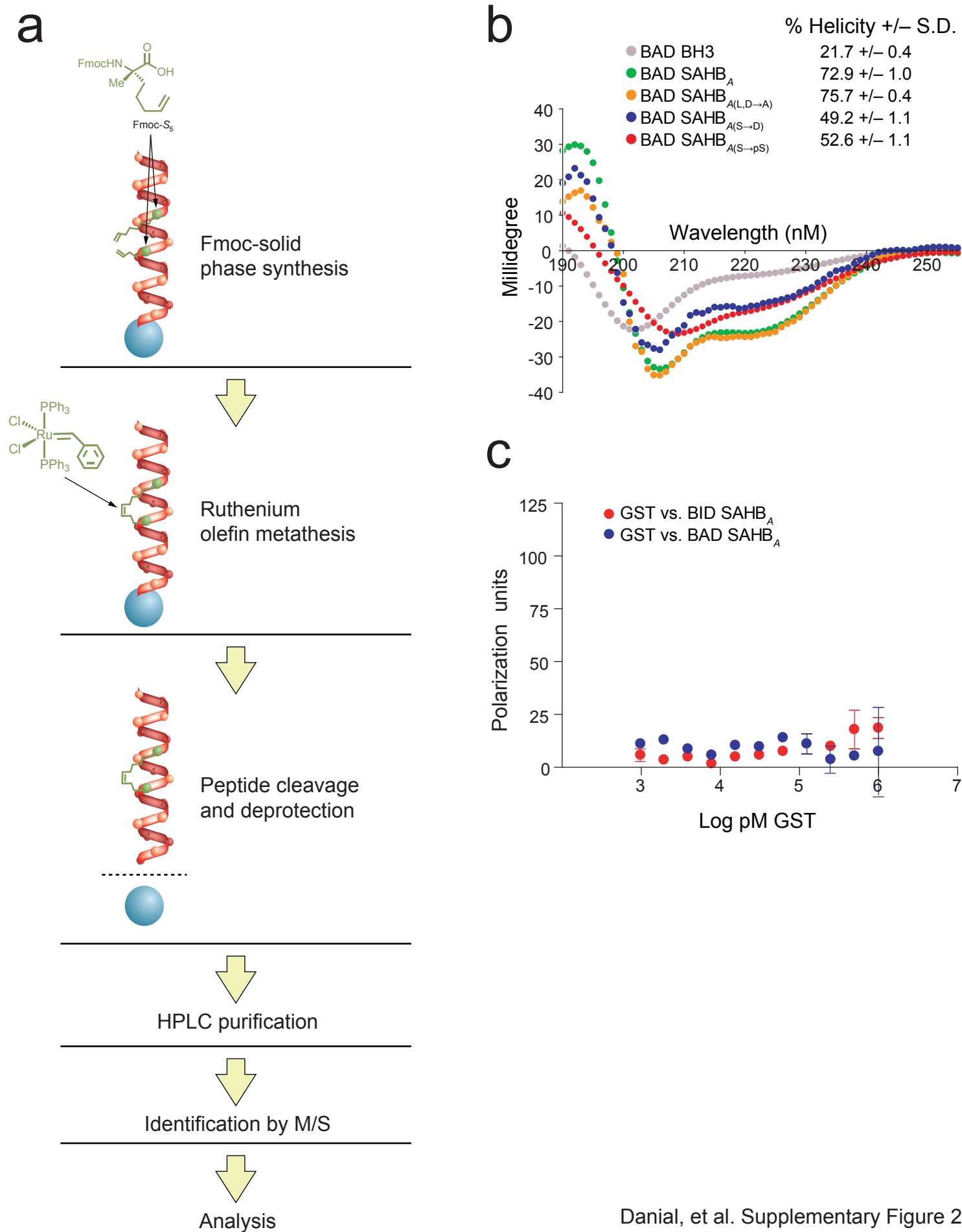
Supplementary Information

Supplementary Figure 1   Association of glucokinase and BAD in beta cells.

a

anti GK   Ctrl
Elution 1st 2nd 3rd   1st 2nd 3rd

WB

GK ▶

BADs ▶

— 21

— 14

1   2   3   4   5   6   (kDa)

b

WB   MC   Ctrl

PP1c ▶

(kDa)

WAVE-1 ▶   — 66

GK ▶

— 46

PKAc ▶

BADs ▶   — 21

Danial, et al. Supplementary Figure 1

Supplementary Figure 1   Association of glucokinase and BAD in beta cells. (**a**) Anti-GK antibody (lanes 1–3) or control rabbit IgG (lanes 4–6) were covalently linked to AminoLink Plus Coupling gel (Pierce) as per manufacturer's instructions and incubated with CHAPS-solubilized mitochondria-enriched heavy membrane (HM) fraction prepared from MIN6 cells. Bound material was sequentially eluted, resolved on SDS-PAGE and immunoblotted (WB) with antibodies to GK or BAD. (**b**) Microcystin affinity purification of PP1-interacting proteins at mitochondria isolated from MIN6 cells. Mitochondria-enriched HM fraction was solubilized in 15 mM CHAPS and incubated with microcystin (MC)-coupled agarose beads[1], bound proteins were resolved by SDS-PAGE and immunoblotted (WB) with the indicated antibodies. Uncoupled beads serve as control (ctrl).

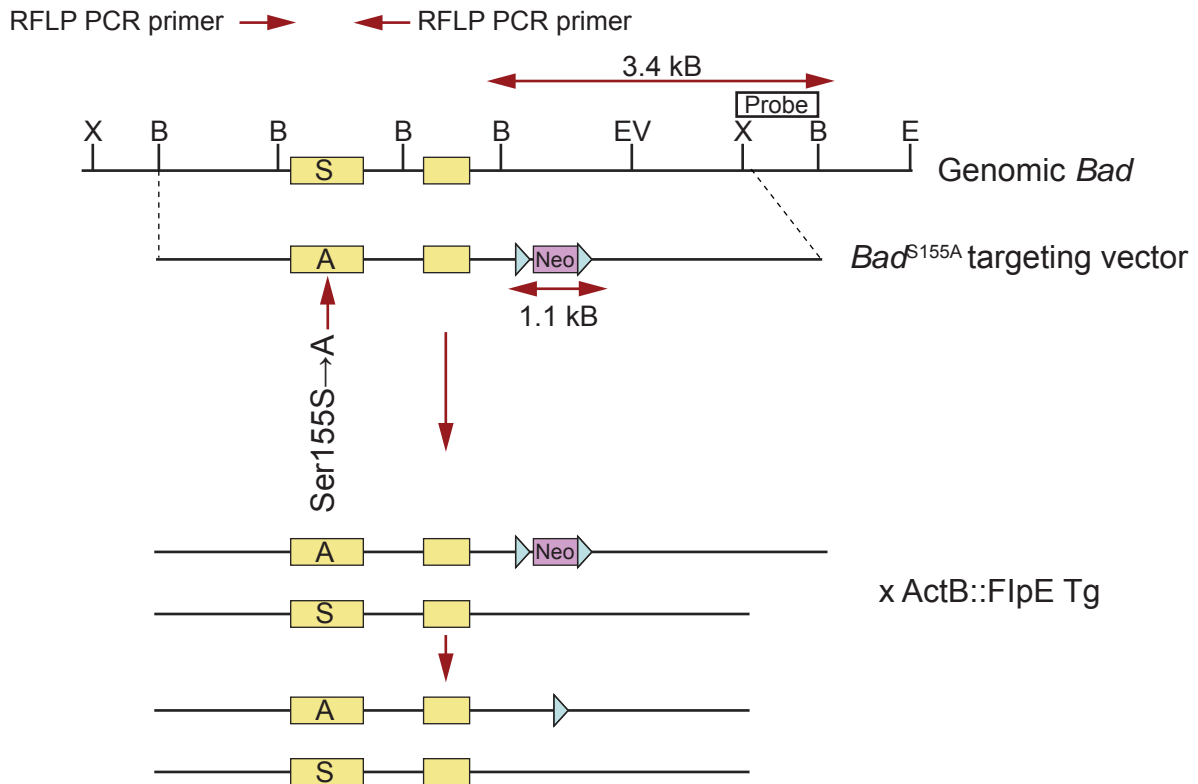Supplementary Figure 2   Generation and characterization of SAHB compounds.

a

FmocHN
Me
O
OH

Fmoc-S_5

Fmoc-solid phase synthesis

Cl
Cl
Ru
PPh3
PPh3

Ruthenium olefin metathesis

Peptide cleavage and deprotection

HPLC purification

Identification by M/S

Analysis

b

% Helicity +/– S.D.

	% Helicity +/– S.D.
BAD BH3	21.7 +/– 0.4
BAD SAHB$_A$	72.9 +/– 1.0
BAD SAHB$_{A(L,D\rightarrow A)}$	75.7 +/– 0.4
BAD SAHB$_{A(S\rightarrow D)}$	49.2 +/– 1.1
BAD SAHB$_{A(S\rightarrow pS)}$	52.6 +/– 1.1

Millidegree

Wavelength (nM)

190   200   210   220   230   250

c

Polarization units

GST vs. BID SAHB$_A$
GST vs. BAD SAHB$_A$

Log pM GST

Danial, et al. Supplementary Figure 2

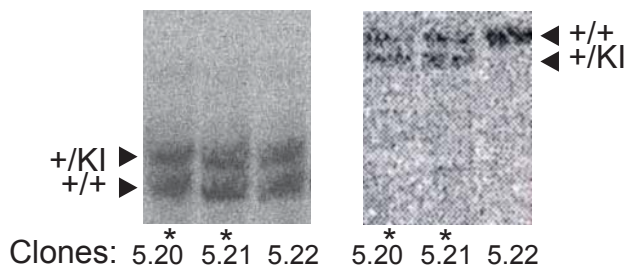**Supplementary Figure 2   Generation and characterization of SAHB compounds.**
(**a**) Schematic of the hydrocarbon-stapling synthetic strategy. Asymmetric synthesis of S-N-(9-Fluorenylmethyl carbamate)-2-(4'-pentenyl)alanine ("S5") was performed as previously described[2,3]. SAHB compounds were generated by replacing two amino acids of the BH3 sequence with non-natural amino acids at discrete locations that flank 3 natural amino acids (i, i+4 positions). Peptide synthesis, olefin metathesis, FITC-derivatization, reverse-phase HPLC purification, and microanalysis were performed as previously reported for BID SAHB[4]. The native methionines of BAD and BID BH3 were replaced with norleucine (N_L) due to the incompatibility of sulfur with the ruthenium-catalyzed metathesis reaction. (**b**) Circular dichroism spectra demonstrate enhanced α-helicity of SAHBs compared to their corresponding unmodified peptides. (**c**) Binding affinities of SAHB compounds to recombinant GST protein, serving as a negative control for binding studies presented in **Fig. 5d**. Fluorescence polarization binding assays were performed using FITC-labeled peptides (50 nM) and control GST protein at the indicated concentrations.

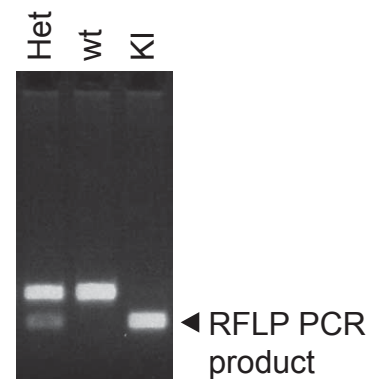Supplementary Figure 3   Generation of Bad^{S155A} knock-in genetic model.

Supplementary Figure 3   Generation of Bad^{S155A} knock-in genetic model.   (a) Knock-in targeting strategy. Map of the BAD locus marks the restriction sites and boxes denote exons. X, Xba1; B, BamH1; EV, $EcoR$V; S, SmaI; E, $EcoR$1. Blue triangles: FRT sites. (**b**) Southern analysis verifying appropriate targeting. The probes indicated in (a) show insertion of the FRT-Neo-FRT cassette (b, left panel) and the integration of the EcoRI RFLP into BAD (b, right panel). Clones marked with (*) were positive for both insert and RFLP. (**c**) PCR fragment for the RFLP mutation marker for BAD S155A after digestion with $EcoR$1, used to genotype the Bad^{S155A} progenies of $Bad^{S155A(neo)/+}$ crossed to FlpE mice. See **Supplementary Methods** for additional details.

Supplementary Figure 4   HFD-induced beta cell mass expansion is BAD-dependent.
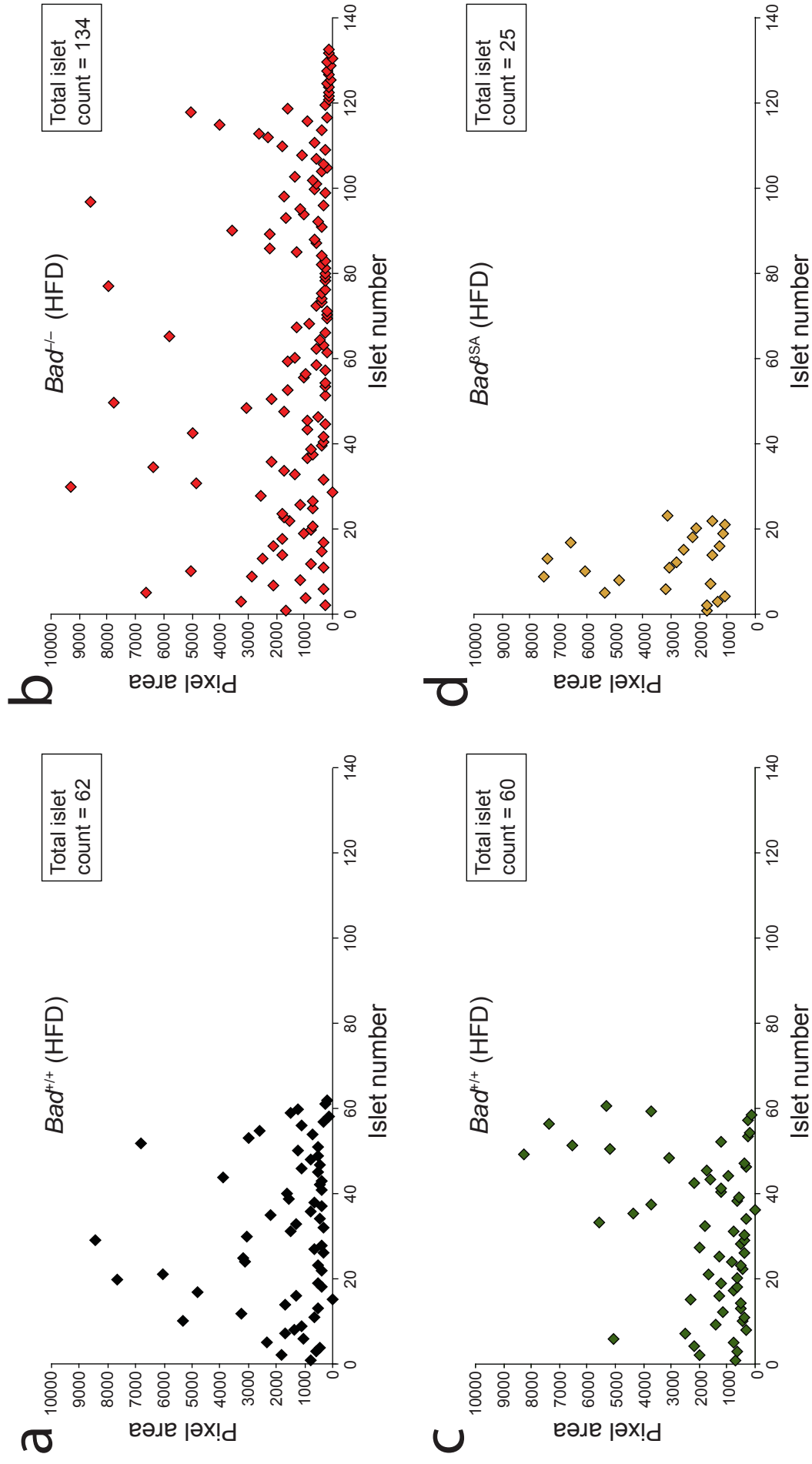
Supplementary Figure 4 HFD-induced beta cell mass expansion is BAD-dependent. Histograms showing the number of islets and their size distribution in representative pancreatic sections prepared from $Bad^{+/+}$ and $Bad^{-/-}$ mice (**a,b**) and $Bad^{+/+}$ and Bad^{3SA} mice (**c,d**) after 16 weeks on HFD. Each diamond represents an islet that was immuno-stained with an antibody to insulin (see **Fig. 6** and Methods).   The vertical axis demonstrates the pixel area assigned to islets traced by the MetaMorph software program. The horizontal axis denotes islets. For each representative pair of genotypes shown ($Bad^{+/+}$ vs. $Bad^{-/-}$ and $Bad^{+/+}$ vs. Bad^{3SA}) the total section area was comparable. $Bad^{-/-}$ sections contain significantly more islets for the same total tissue area, while Bad^{3SA} mice have significantly fewer islets. Multiple sections from at least 3 animals per group were analyzed in a similar fashion.

Supplementary Table 1 Quantitative analysis of $[Ca^{2+}]_i$ responses in *Bad*$^{+/+}$ and *Bad*$^{-/-}$ islet cells.

	Bad$^{+/+}$ (n=116)	*Bad*$^{-/-}$ (n=115)
Basal $[Ca^{2+}]_i$ at 3 mM glucose (F340/F380)	0.74 ± 0.01	0.72 ± 0.01 n.s.
Average $[Ca^{2+}]_i$ response to 11 mM glucose (F340/F380)	1.40 ± 0.04	0.89 ± 0.03 ***
Average height of peaks above baseline (amplitude) (F340/F380)	1.10 ± 0.04	0.62 ± 0.02 ***
Average $[Ca^{2+}]_i$ response to 35 mM KCl (F340/F380)	1.95 ± 0.07	1.98 ± 0.05 n.s.

Supplementary Table 1 Quantitative analysis of $[Ca^{2+}]_i$ responses in *Bad*$^{+/+}$ and *Bad*$^{-/-}$ islet cells.   Analysis was performed using the Ion Wizard software (IonOptix). Representative traces of this experiment are shown in **Fig. 3b-g**. Similar results were obtained for 16.7 mM glucose (data not shown). n.s.: not significant, *** $P < 0.001$.

SUPPLEMENTARY METHODS

Generation of *Bad*^{S155A} mice. We introduced the S155A mutation in the BAD BH3 domain with silent RFLP encoding an *Eco*R1 site into *Bad* exon 3 by QuickChange using pBR322BAD as template. We swapped a 900 bp *Sex*A1/*Rsr*II fragment containing this mutation into a new pBR322BAD construct. We cloned an FRT-PGK-NEO-FRT cassette into an *Nsi*I site 1.4 kB distal to the BAD 3'UTR, and introduced a diphtheria toxin-negative selection cassette into genomic *Bad*/pBR322 junction at the 5' end of the *Bad* locus. We electroporated this vector into 129 J1 ES cells and injected it into C57B6 blastocysts. We identified and verified homologous recombinants by standard procedures (**Supplementary Fig. 3**). We re-isolated the *Sex*A1/ *Rsr*II fragment from mice positive for the RFLP marker and sequenced to verify that the mice carried the correct mutation. We excised the NEO cassette after generation of the *Bad*$^{S155A(neo)/+}$ by crossing to FlpE transgenic mice.

Metabolic studies. We performed hyperglycemic clamp studies following the standardized procedures established at the Yale University Mouse Metabolic Phenotyping Center. At least 5 days before the clamp analysis, we anesthetized 10 week-old male mice and inserted an in-dwelling catheter into the right internal jugular vein for intravenous infusion of glucose. Clamp analysis was conducted on overnight fasted mice in awake and minimally-stressed state. We attached a 3-way connector to the jugular vein catheter for intravenous infusion and obtained blood samples. We conducted a 2-hour hyperglycemic clamp with a primed and variable infusion of 20% glucose to raise and maintain plasma glucose concentrations at ~300 mg/dl. We collected blood samples (20 μl) at 10–20 min intervals for the immediate measurement of plasma glucose concentrations using the Beckman Glucose Analyzer II (Beckman). We measured plasma insulin by radioimmunoassay (Linco Research).

Insulin secretion studies. We routinely cultured the Islets for 1-2 days prior to perifusion or static incubation assays. We performed islet perifusion assays as previously described[5]. Briefly, we placed 120 islets in a column between two layers of Cytodex-3

micro-carrier beads (Pharmacia) and perifused with Krebs buffer [119 mM NaCl, 4.6 mM KCl, 1 mM $MgSO_4$, 0.15 mM Na_2HPO_4, 0.4 mM KH_2PO_4, 25 mM $NaHCO_3$, 2 mM $CaCl_2$, 20 mM HEPES (pH 7.4), 0.05% (wt/vol) BSA] containing the indicated concentration of glucose or KCl. We pumped the perifusion solution using a high precision multi-channel pump (IP Istamec model #78023-02, Cole-Parmer Instruments) at a flow rate of 0.3 ml/min to ensure islets were not exposed to excessive pressure during the course of perifusion. Prior to fraction collection, we perifused islets with 3 mM glucose for 25 min. We collected the eluted fractions every 15 sec using a BioRad fraction collector (Model #2128). We maintained the entire system in a chamber at 37°C. We changed the glucose concentration in perifusion solution at the indicated times (**Fig. 2a**). We measured insulin by radioimmunoassay.

For static incubation (batch release) assays, we washed the islets 3 times and picked 5 islets per tube in Krebs buffer containing 3 mM glucose followed by 30 min incubation at 37°C. We pelleted the islets and replaced the buffer with Krebs solution containing the indicated concentration of glucose or secretagogues. For each glucose or secretagogue concentration, we analyzed 10–12 tubes. After 1 hour incubation at 37°C, we pelleted the islets and collected the supernatant for insulin measurement. We solubilized the pellet to assess intracellular insulin content. Insulin was measured by ELISA using mouse insulin as a standard (Insulin ELISA Kit, cat. #INSKR020, Crystal Chem).

Glucokinase assays in primary islets and INS-1 cells. We performed the assays in 96 well format using a SpectraMax M5 plate reader (Molecular Devices). Briefly, we homogenized ~900–1000 mouse islets (**Fig. 2e**) or 5–6 x 10^6 INS-1 cells (**Fig. 5e**) in buffer containing 30 mM Tris-HCl (pH 8.2), 4 mM EDTA, 150 mM KCl, 4 mM $MgCl_2$, 2.5 mM DTT, 1 mM 5'-AMP, 3mM Potassium Phosphate (pH 7.4), 1 mM K_2SO_4, 15 mM β- mercaptoethanol and 0.2% BSA, using a Teflon pestle and a rotary homogenizer[6]. We saved a small aliquot of homogenates for DNA or protein content measurement. We detected glucose phosphorylating activity in a glucose-6-phosphate dehydrogenase (G6PDH)-driven NADH production reaction. We calculated glucokinase activity as the

difference in NADH produced at glucose concentrations of 100 mM (glucokinase activity) and 0.5 mM (hexokinase activity) in a reaction buffer that in addition to glucose contained 50 mM HEPES HCl (pH 7.7), 100 mM KCl, 7.4 mM $MgCl_2$, 15 mM β-mercaptoethanol, 0.5 mM NAD^+, 0.05% BSA, 2.5 μg/ml (0.7 U/ml) G6PDH (sigma) and 5 mM ATP. We performed the reactions for 90 min at 31°C in a total volume of 100 μl. The values routinely obtained in these assays are within range of those previously reported[6].

Measurement of mitochondrial membrane potential. After dispersion, we plated the islets on coverslips followed by overnight incubated at 37°C. On the day of experiment, we pre-incubated the cells in 3 mM glucose for 3 hours. Prior to imaging, we loaded the cells with 7 nM tetramethyl rhodamine ethyl ester (TMRE) and 100 nM MitoTracker Green (MTG) (Invitrogen) for 45 min and 30 min, respectively. We removed the MTG from the media and imaged the cells using an inverted Leica TCS SP2 confocal microscope (Wetzlar). We obtained four stacked images from multiple individual cells before and after raising the extracellular glucose concentration from 3 mM to 8 mM or before addition of 10 mM KIC. We analyzed the TMRE fluorescence as described previously[7,8].

Circular dichroism. We dissolved the SAHB peptides in water at neutral pH to concentrations of 25–50 μM. We obtained CD spectra on a Jasco J-710 spectropolarimeter at 20°C using the following standard measurement parameters: wavelength, 190–260 nm; step resolution, 0.5 nm; speed, 20 nm/sec; accumulations, 10; response, 1 sec; bandwidth, 1 nm; path length, 0.1 cm. The α-helical content of each peptide was calculated from the mean residue molar ellipticity value at 222 nm ($[θ]222$)[9,10].

Fluorescence polarization assays (FPA). We performed FPA using a glutathione S-transferase fusion protein of BCL-X_L (residues 1−212) lacking the C-terminal transmembrane domain (GST-BCL-X_L ΔC), which was expressed in *E. coli* BL21 using pGEX2T (Pharmacia Biotech), and purified by affinity chromatography using

glutathione-agarose beads (Sigma) and fast protein liquid chromatography (FPLC). We determined the protein concentration using the Bradford Assay. We incubated the fluorescinated SAHBs (50 nM) with GST-BCL- X_L ΔC (0.25–1000 nM) or GST control protein in binding buffer [(140 mM NaCl, 50 mM Tris-HCl (pH 7.4)] at room temperature. We measured binding activity by fluorescence polarization using a POLARstar OPTIMA microplate reader (BMG labtech). We determined the EC_{50} values by nonlinear regression analysis using Prism software (Graphpad).

Real-time PCR. We prepared total RNA from islets using the Rneasy Plus Mini Kit (Qiagen). We used at least three separate animals for RNA preparations and prepared the RNA samples in duplicate or triplicate and performed control cDNA synthesis reactions containing no reverse transcriptase enzyme for each sample. We ran the PCR reactions in triplicates. We used 1 μg of total RNA in 20 μl cDNA synthesis reactions using standard techniques. We diluted the cDNA 20 fold and used 2 μl in a 25 μl PCR reaction using primers for BAD. Another set of control reactions contained primers for ribosomal protein (RPL4), which served as an internal control for the quality of RNA. Reaction mixture contained 300 nM of each primer and 1X SYBR Green PCR Master Mix (Applied Biosystems). We detected the PCR products with the ABI Prism 7700 Sequence Detector (Applied Biosystems) and determined the threshold values (C_T) as a measure of the cycle number at which a statistically significant increase in fluorescence intensity is first detected. We calculated the abundance of the amplified gene using C_T values and normalized to the average values of RPL4 to obtain relative abundance. We then normalized the relative abundance to that of $Bad^{+/+}$ samples and plotted the ratios. The sequence of primers is available upon request.

Histological analysis and islet area measurements. We prepared serial 5-μm pancreatic sections from pancreata that were fixed in 10% formalin and embedded in paraffin. We stained the sections using a guinea pig antibody to human insulin #4011-01 (Linco Research), followed by incubation with peroxidase conjugated AffiPure secondary antibodies (Jackson Immuno Research). We developed the sections using 3,3-diaminobenzidine tetrahydrochloride and then counterstained with hematoxylin and

eosin. For islet area measurements, we stained the sections with antibody to insulin followed by biotinylated secondary antibody and labeled with Texas Red conjugated streptavidin (Molecular Probes). For each section, we captured digital images of 14 low magnification fields on average, which were then analyzed using the MetaMorph software. Briefly, we traced and thresholded the islets from each section using the MetaMorph software and calculated the insulin positive area. We divided the sum of insulin positive area (total islet area) by the total tissue area on each slide and expressed the value as percentage islet area. Multiple sections from 3–5 mice per group were analyzed.

SUPPLEMENTARY REFERENCES

1. Danial, N.N.*, et al.* BAD and glucokinase reside in a mitochondrial complex that integrates glycolysis and apoptosis. *Nature* **424**, 952-956 (2003).
2. Schafmeister, C., Po, J. & Verdine, G. An all-hydrocarbon cross-linking system for enhancing the helicity and metabolic stability of peptides. *J Am Chem Soc* **122**, 5891-5892 (2000).
3. Williams, R.M. & Im, M.N. Asymmetric synthesis of monosubstituted and alpha, alpha-disubstituted amino acids via diastereoselective glycine enolate alkylations. *J Am Chem Soc* **113**, 9276-9286 (1991).
4. Walensky, L.D.*, et al.* Activation of apoptosis in vivo by a hydrocarbon-stapled BH3 helix. *Science (New York, N.Y* **305**, 1466-1470 (2004).
5. Cunningham, B.A., Deeney, J.T., Bliss, C.R., Corkey, B.E. & Tornheim, K. Glucose-induced oscillatory insulin secretion in perifused rat pancreatic islets and clonal beta-cells (HIT). *Am J Physiol* **271**, E702-710 (1996).
6. Trus, M.D.*, et al.* Regulation of glucose metabolism in pancreatic islets. *Diabetes* **30**, 911-922 (1981).
7. Heart, E., Corkey, R.F., Wikstrom, J.D., Shirihai, O.S. & Corkey, B.E. Glucose-dependent increase in mitochondrial membrane potential, but not cytoplasmic calcium, correlates with insulin secretion in single islet cells. *American journal of physiology* **290**, E143-E148 (2006).
8. Wikstrom, J.D.*, et al.* beta-Cell mitochondria exhibit membrane potential heterogeneity that can be altered by stimulatory or toxic fuel levels. *Diabetes* **56**, 2569-2578 (2007).
9. Chen, Y.H., Yang, J.T. & Chau, K.H. Determination of the helix and beta form of proteins in aqueous solution by circular dichroism. *Biochemistry* **13**, 3350-3359 (1974).
10. Yang, J.T., Wu, C.S. & Martinez, H.M. Caculation of protein conformation from circular dichroism. *Methods Enzymol* **130**, 208-269 (1986).